# Diagnostic analysis of ozone concentrations simulated by two regional-scale air quality models

Jerold A. Herwehe*, Tanya L. Otte, Rohit Mathur, and S. Trivikrama Rao

Atmospheric Modeling and Analysis Division, National Exposure Research Laboratory,
Office of Research and Development, U.S. Environmental Protection Agency
Research Triangle Park, NC 27711, USA

Revised 19 July 2011

Submitted to *Atmospheric Environment*

*Corresponding author. U.S. Environmental Protection Agency, 109 T.W. Alexander Dr., Mail Drop E243-01, Research Triangle Park, NC 27711. Tel.: +1 919 541 0166; fax: +1 919 541 1379.
*E-mail address:* herwehe.jerry@epa.gov (J. Herwehe)

**Abstract**

Since the Community Multiscale Air Quality modeling system (CMAQ) and the Weather Research and Forecasting with Chemistry model (WRF/Chem) use different approaches to simulate the interaction of meteorology and chemistry, this study compares the CMAQ and WRF/Chem air quality simulation results for a month-long retrospective study period (August 2006) over the eastern United States, including comparisons with data from several observation networks. To help improve the comparability of the two models, the 2005 Carbon Bond chemical mechanism (CB05) was implemented into WRF/Chem. In addition, the same emissions, initial and boundary conditions have been used in both models to inter-compare simulated ozone ($O_3$) from the WRF-driven CMAQ and WRF/Chem models. Results reveal that ground-level $O_3$ from both models is biased high, especially in the central South and Ohio River Valley; however, WRF/Chem predicts roughly 10% more $O_3$ aloft (1000-2500 m AGL) than CMAQ. Different model configurations due to the choice of land surface model (LSM), planetary boundary layer (PBL) physics scheme, and convective cloud parameterization contributed to the differences seen in simulated $O_3$, but most important were the different treatments of the radiative effects of clouds by their respective photolysis schemes.

**Keywords**

CMAQ, WRF/Chem, ozone, air quality model, model evaluation, model intercomparison

## 1. Introduction

For the past decade, the Community Multiscale Air Quality modeling system (CMAQ; Byun and Schere, 2006) has been an offline chemical transport model driven by meteorological fields from models such as the Weather Research and Forecasting model (WRF; Skamarock and Klemp, 2008). During this decade, CMAQ has built a worldwide community of several thousand users who have successfully employed the modeling system for a variety of research, regulatory, forecasting, and climate applications.

However, offline chemistry does not allow aerosol feedbacks from the chemical transport model to affect the radiation budget, cloud microphysics, and precipitation in the meteorological model. Such feedbacks are particularly important in light of the increased focus on the interactions of air quality and climate change. An alternative approach is to use an online coupled chemistry and dynamics model, such as the WRF with Chemistry model (WRF/Chem; Grell et al., 2005) or the coupled WRF-CMAQ system (Mathur et al., 2010) because they treat the physical and chemical feedback processes. However, regional-scale online modeling is relatively new (Zhang, 2008), and there are still many unresolved issues related to the simulation of aqueous chemical processes in an online system. This deficiency affects the online system's ability to properly handle the physical feedback mechanisms. In addition, online systems require increased computational resources to run both the meteorology and chemistry modules concurrently, which may render the online systems impractical for some research and regulatory groups. Thus, both offline and online modeling systems will continue to be used for various applications for some time.

This study presents a diagnostic analysis of Eulerian (i.e., grid-based), limited-area offline and online meteorology and chemistry modeling systems. Here, the WRF-driven CMAQ modeling system and the WRF/Chem model are compared by analyzing simulated ozone ($O_3$) for a summer month (August 2006) and selected physical and chemical processes that are responsible for differences in modeled $O_3$ at the surface and aloft. The object of this intercomparison is not to determine which modeling system (offline WRF-CMAQ vs. online WRF/Chem) is most skillful in reproducing the observations. Rather, it is to diagnose and understand the differences between the two modeling systems, to identify strengths and weaknesses of the systems, and to inform future development to improve the simulation of air quality (AQ) by both systems.

## 2. Modeling configuration and approach

The 2008 versions of the two air quality modeling systems were used for this intercomparison study. CMAQ v4.7 was driven by WRF-ARW v2.2 (WRF-for-CMAQ in this paper) which included additional physics packages that were later released in v3.0 (Gilliam and Pleim, 2010). The 2005 update to the Carbon Bond mechanism (CB05; Yarwood et al., 2005) was implemented into WRF/Chem v3.0.1.1 to conduct a more compatible comparison of gas phase chemistry results with the CMAQ modeling system. In addition, CB05 was coupled to WRF/Chem's Modal Aerosol Dynamics model for Europe (MADE; Ackermann et al., 1998) and Secondary Organic Aerosol Model (SORGAM; Schell et al., 2001) schemes to allow direct and indirect aerosol feedback to the shortwave (SW) radiation and cloud microphysics. Specialized software converted CMAQ-ready initial and boundary conditions (ICs/BCs) and CB05-speciated emissions for WRF/Chem to enable both systems to use the same initial, lateral boundary, and emissions forcing. Hourly meteorological input data for offline ingestion by CMAQ were prepared from the WRF output by the Meteorology-Chemistry Interface Processor (MCIP; Otte and Pleim, 2010). CMAQ then linearly interpolated the hourly meteorological input data for each model time step (e.g., every five minutes) during the CMAQ simulation. In contrast, the online coupled WRF/Chem drove its chemistry with meteorological values from every model time step (every minute for this study), thereby allowing temporally nonlinear changes in the meteorology within each hour to more realistically affect the transport, mixing, and effective reaction rates of the chemical species.

The input fields and geophysical dimensions of the offline and online modeling systems were set to be as similar as possible (Table 1), but each modeling system was allowed to use the physics options in the meteorological module that are typically recommended by the developers of the AQ models (Table 2). The modeling domain covered the eastern United States with 12-km horizontal grid cells with vertical extent to 100 hPa using 34 terrain-following layers and the lowest layer is 35-m thick. A month-long period was chosen for this study to permit robust statistical analyses on the regional scale. August 2006 was selected because of expected summer season high $O_3$ values and a partial overlap with the observational period of an intensive field campaign conducted around Houston, Texas. Meteorological ICs/BCs originated from the National Centers for Environmental Prediction (NCEP) North American

Mesoscale model (NAM), which also provided fields for four-dimensional data assimilation (FDDA), as documented by Gilliam and Pleim (2010). Chemical ICs/BCs were created from a CMAQ simulation for the same period but which used 36-km horizontal grid spacing (Foley et al., 2010). Anthropogenic emissions were projected to 2006 from the 2001 U.S. Environmental Protection Agency's (USEPA's) National Emissions Inventory (NEI; http://www.epa.gov/ttn/chief/net/critsummary.html) and include mobile emissions from the Mobile6 emissions model (http://www.epa.gov/otaq/m6.htm). The biogenic emissions were processed using the Biogenic Emissions Inventory System (BEIS) v3.13. WRF, CMAQ, and WRF/Chem were initialized at 00 UTC 29 July 2006 to allow for a three-day spin-up period for the chemical processes, and this spin-up period is not used in the analyses described later in this paper.

Table 2 also lists differences in the recommended near-surface physics options for each modeling system. WRF-for-CMAQ and CMAQ utilized the Pleim-Xiu (PX) LSM, the Pleim surface layer scheme, and the Asymmetric Convective Model version 2 (ACM2) PBL scheme, while WRF/Chem used the NCEP – Oregon State University – Air Force – Hydrologic Research Laboratory (Noah) LSM, Monin-Obukhov surface layer, and Yonsei University (YSU) PBL schemes. The important effects of these choices are described later as appropriate during the discussion of the results and analyses.

The Rapid Radiative Transfer Model (RRTM) used in both modeling systems for longwave (LW) radiation processes considers cloud optical depth; and distributions of water vapor, $O_3$, carbon dioxide ($CO_2$), and other trace gases, such as methane ($CH_4$) and nitrous oxide ($N_2O$), if available. Neither modeling system treats the effects of prognostic aerosols on LW radiation. However, both modeling systems simulate the direct effects of scattering and absorption on SW radiation and photolysis due to resolved water vapor and cloud droplets. In addition, WRF/Chem allows for direct feedback effects from parameterized subgrid convective precipitation and prognostic aerosols on the SW radiation and the photolysis rates. WRF/Chem also allows some indirect feedbacks on radiation and cloud microphysics by computing a prognostic cloud droplet number, though there are no aerosol indirect effects from the MADE/SORGAM scheme in this version of WRF/Chem.

153 Photolysis in CMAQ is a two-step process. First, an offline preprocessor ("JPROC") computes
154 clear-sky climatological photolysis rates as a function of zenith angle, latitude, altitude, and chemical
155 mechanism using prescribed aerosol and interpolated seasonal $O_3$ profiles. Second, an online routine
156 ("PHOT") then dynamically corrects the preprocessed photolysis rates according to parameterized
157 estimates of cloud cover during the simulation (Roselle et al., 1999). Because JPROC is offline, it does
158 not consider any attenuation by prognostic aerosol parameters during the simulation. The online Fast-J
159 photolysis scheme (Wild et al., 2000) used by WRF/Chem is coupled to the hydrometeor, aerosol, and
160 convective cloud parameterizations to account for scattering and absorption along the optical path.
161

162 **3. Evaluation of simulated ground-level ozone**

163

164 *3.1. Comparison of model results with surface observations*

165

166 Surface measurements used for evaluation of the model results were acquired from two different
167 databases: the USEPA's Air Quality System (AQS; http://www.epa.gov/ttn/airs/airsaqs/) and the
168 SouthEastern Aerosol Research and Characterization study (SEARCH; http://www.atmospheric-
169 research.com/studies/SEARCH/index.html). The simulated concentrations in the lowest model layer
170 (layer 1, approximately 35 m thick) are used for comparisons with surface observations.
171

172 *3.1.1. Modeled ozone compared with AQS data*

173 Statistics for the daily maximum 8-h average $O_3$ for August 2006 were generated by the
174 Atmospheric Model Evaluation Tool (AMET; Appel et al., 2011) for each of the two AQ modeling
175 systems by comparing with archived quality assured and quality controlled hourly $O_3$ data from AQS sites
176 within the grid cells. Selected statistics from this analysis, shown in Table 3, reveal that both models are
177 biased high when predicting surface $O_3$ for the month of August 2006, but CMAQ's predictions are in
178 slightly better agreement with observations than WRF/Chem's.

The diurnal variations in $O_3$ for the domain-wide AQS observations and the CMAQ and WRF/Chem models indicate the general overprediction by each model, especially during nighttime hours (Fig. 1). Despite some overestimation, model results and observations are closer during the 1-2-hour morning transition to daytime convective conditions, with a 1-h phase lag by both models to begin the morning increase in surface $O_3$. Fig. 1 also shows that the WRF/Chem surface $O_3$ exhibits some phase lag during the afternoon and evening, reaching its peak $O_3$ values about one hour after CMAQ and the observations, and showing a slower decay of $O_3$ in the evening. This behavior is likely due to the more vigorous vertical mixing of WRF/Chem's YSU scheme, especially during stable conditions when YSU's stronger downward heat flux (Hu et al., 2010) would delay the collapse of the PBL.

To examine spatial relationships, Fig. 2 displays full month-averaged August 2006 surface $O_3$ mixing ratios and differences for both modeling systems with the available AQS site averages overlaid along with the NMB for modeled $O_3$ at each AQS site. Both models are biased high in the southeastern U.S. (hereafter SE), but the $O_3$ overprediction by WRF/Chem is more pronounced and extends into the Ohio River Valley (ORV), northward along the Appalachians, and northwestward into Minnesota (Figs. 2b and e). This may be due to the nocturnal transport of larger amounts of ozone trapped aloft in the residual layer by WRF/Chem. The month-averaged AQS data (Fig. 2) showed relatively low $O_3$ mixing ratios, influenced by low nocturnal $O_3$ observations which, as was seen in Fig. 1, the models had difficulty achieving. To examine the contributions of different periods of the day to the month-averaged $O_3$, month-long averages were produced for three selected daily time periods, each consisting of four hourly values (or 124 hourly values for each average): local time nocturnal conditions (06-09 UTC), local morning conditions (11-14 UTC), and local afternoon conditions (17-20 UTC). Month-averaged morning and afternoon periods are shown in Fig. 3 for surface $O_3$ and differences with the correspondingly-averaged AQS $O_3$ data overlaid. WRF/Chem's inability to reduce surface $O_3$ as rapidly as CMAQ overnight was evident in the nocturnal-averaged $O_3$ (not shown). By the morning hours, WRF/Chem's $O_3$ has decreased noticeably, but is still biased high in the central South and southern Appalachians (Fig. 3b). Relatively significant $O_3$ advection is evident over water off the Eastern

205 Seaboard for CMAQ (Figs. 3a and d), but no observations are available over water for verification. In the
206 afternoon, WRF/Chem tended to underestimate $O_3$ in the western Plains states and further west, but
207 showed significant overestimation of $O_3$ in the SE and ORV (Fig. 3e). As seen in the month-average and
208 morning $O_3$ differences (Figs. 2c and 3c), CMAQ continued to have significantly more $O_3$ than
209 WRF/Chem in the afternoon over areas likely to be stably stratified, such as over ocean waters and the far
210 western Plains and Rocky Mountains (Fig. 3f). Figures 1 and 3 show that AQ modeling systems are
211 better at predicting the high afternoon $O_3$ mixing ratios than the lower nighttime values. Reduced vertical
212 mixing during stable nocturnal conditions leads to a significant vertical gradient close to the ground since
213 $O_3$ continues to decrease due to dry deposition and titration by its reaction with NO and the resultant low
214 observed surface $O_3$ mixing ratios are not represented well owing to the models' 35-m thick lowest layer.
215
216 *3.1.2. Ozone chemistry characteristics at selected SEARCH sites*
217 To gain some insight into the $O_3$ chemical production in the August 2006 air masses in the SE,
218 net ozone production efficiency (OPE) and air mass photochemical age were computed at selected
219 SEARCH sites using results from the two AQ modeling system and from SEARCH observations for
220 comparison. The two SEARCH sites discussed here represent different land use patterns and proximity to
221 emissions sources: Centreville, AL (rural, forest; 32.90289° N, 87.24968° W, 126 m MSL) and
222 Birmingham, AL (urban, industrial-residential; 33.55303° N, 86.81482° W, 177 m MSL), referred to as
223 CTR and BHM, respectively, in this paper. The hourly SEARCH trace gas measurements for $O_3$, nitric
224 oxide (NO), nitrogen dioxide ($NO_2$), and total reactive nitrogen ($NO_y$) were used in this study.
225 OPE is defined as the amount of $O_3$ produced for each molecule of nitrogen oxides ($NO_x$; where
226 $NO_x = NO + NO_2$) consumed and is indicated by the relationship of $O_3$ to the $NO_x$ photooxidation
227 products surrogate, $NO_z$, defined by $NO_z = NO_y - NO_x$. Although $NO_y$ was one of the measured
228 quantities at the SEARCH sites, $NO_y$ is not typically provided in AQ model output. Therefore, from the
229 CB05 chemical mechanism, $NO_y$ is defined as
230

$$NO_y = NO + NO_2 + NO_3 + 2N_2O_5 + HONO + HNO_3 + PAN + PANX + PNA + NTR \quad (1)$$

where $NO_3$ is the nitrate radical, $N_2O_5$ is dinitrogen pentoxide, HONO is nitrous acid, $HNO_3$ is nitric acid, PAN is peroxyacetyl nitrate, PANX is C3 and higher peroxyacyl nitrates, PNA is peroxynitric acid, and NTR is organic nitrate (Yarwood et al., 2005). Once $NO_x$, $NO_y$, and $NO_z$ were calculated, OPE was then determined from a linear regression fit of $O_3$ versus the $NO_z$ distribution binned in 5% intervals for the daytime hours of 10:00-17:00 local standard time (LST) following the technique of Olszyna et al. (1994). As described in Olszyna et al., the binning of $NO_z$ facilitates visualizing data relationships by indicating the frequency distribution of the data. Because differential dry deposition rates between $O_3$ and the $NO_z$ species were not considered, the net OPE presented here should be considered upper bounds.

The value of "SLOPE" shown in each $O_3$ v. $NO_z$ plot of Fig. 4 gives the OPE as determined by the regression fit for August 2006. At these selected sites, OPE values from the SEARCH observations range from 10.32-23.67, while OPE values from the two models range from 3.22-6.03, with the WRF/Chem OPE values noticeably smaller than those of CMAQ. In simulations of summer 2002 using CMAQ with the CB4 mechanism, Godowitch et al. (2008) also reported that model-based OPE was significantly less than observation-based OPE at many SEARCH sites. For August 2006, CMAQ and WRF/Chem exhibit less potential for $O_3$ production at CTR and BHM (less than half as much as observed), and yet have positive $O_3$ biases compared with the AQS observations as seen previously in Figs. 2 and 3. A plausible explanation is that the models produce $O_3$ too rapidly from the available $NO_x$ and organic carbon precursors and then underestimate processes for $O_3$ loss, such as too little dry deposition, thus allowing $O_3$ to accumulate and maintain relatively high values despite relatively low OPE in the models.

According to Olszyna et al. (1994), a measure of air mass photochemical age can be provided by $1 - (NO_x/NO_y)$, which is the fraction of the initial $NO_x$ emissions that have been converted to photooxidation products, thereby providing some indication of whether the air parcel is fresh or aged. Air masses are considered to be chemically mature when their air mass photochemical age values are greater

than 0.6 (Trainer et al., 1993). The percentage of August 2006 data at the two Alabama SEARCH sites that can be considered photochemically-aged is as follows: at CTR, SEARCH = 80% (Fig. 5a), CMAQ = 100% (Fig. 5b), WRF/Chem = 100% (Fig. 5c) and at BHM, SEARCH = 10% (Fig. 5d), CMAQ = 45% (Fig. 5e), WRF/Chem = 60% (Fig. 5f). The rural site (CTR) is far enough removed from fresh emissions that most air masses moving over CTR are chemically mature with much of their original $NO_x$ photooxidized. In contrast, the urban BHM site indicates its proximity to fresh emissions with fewer aged air masses passing through. The modeled air masses for these sites are clearly more aged than shown by the observations. Because the mid-day modeled air is more aged, it is less efficient in producing $O_3$ (Figs. 4 and 5). These results are also likely due to the model reactions taking place over a relatively large grid cell volume which dilutes extreme values, while the observation network sites may be influenced by local emissions and finer-scale features that are unresolved by the models.

*3.2. Comparison of key processes affecting surface ozone*

Differences in modeled physical processes caused differences in simulated surface $O_3$ despite the similar chemical conditions (i.e., the same chemical mechanism, emissions, and ICs/BCs) used by the two modeling systems. The month-averaged $O_3$ difference plot of Fig. 2c revealed systematic differences in how each model treated metropolitan areas, and also showed that, on average, WRF/Chem has 7-11 ppbv more $O_3$ than CMAQ in many areas of the central South, Appalachians, and ORV, while CMAQ has similar greater amounts of $O_3$ than WRF/Chem in many areas in the eastern Rocky Mountains and over water off the coasts. The corresponding month-averaged PBL heights from WRF-for-CMAQ and WRF/Chem (Figs. 6a and b, respectively) and their differences (Fig. 6c) show the generally deeper average PBLs for WRF/Chem everywhere, especially in the western Plains and west Texas. Analysis of the monthly-averaged 2-m temperature and water vapor mixing ratio (not shown) revealed that WRF/Chem with its Noah LSM and YSU PBL scheme was generally biased warmer and drier than WRF-for-CMAQ with its PX LSM and ACM2 PBL scheme, especially in the South and Plains states, which

would contribute to the deeper PBLs seen in the WRF/Chem simulation. This is corroborated by Hu et al. (2010) which reported that at night ACM2 produces greater static stability near the surface than YSU, but that the stronger nighttime thermal and moisture fluxes of YSU lead to low-level temperatures and moisture closer to observations. The metropolitan areas are not as apparent in the PBL height differences (Fig. 6c), which is likely due to the displayed difference scale range. Month-averaged surface carbon monoxide (CO) and its differences between the models (not shown) revealed that CMAQ had significantly greater CO mixing ratios over metropolitan areas than WRF/Chem, indicating less dilution over CMAQ's urban areas. Similar plots for NO (not shown) support the idea that titration of $O_3$ by higher NO mixing ratios in CMAQ could be the cause for lower $O_3$ in its urban areas compared to WRF/Chem. From the generally deeper PBLs generated by WRF/Chem, one would expect that, because of dilution, WRF/Chem's surface $O_3$ would be less than that from WRF-driven CMAQ, but that is not the case in the eastern half of the U.S.

Average afternoon (17-20 UTC) PBL heights with differences (Fig. 7) are similar to the pattern for the full-month PBL averages (Fig. 6), but normalized afternoon PBL height differences are generally smaller in magnitude (note that Fig. 7 has double the scale range of Fig. 6), mixing afternoon $O_3$ through relatively more similar PBL heights. The parameterization of convection in the ACM2 and YSU PBL schemes both account for nonlocal mixing, thus reducing the impact of urban areas on afternoon $O_3$ mixing ratios. However, model difference plots of average afternoon CO and $NO_2$ (not shown) still show CMAQ with higher mixing ratios than WRF/Chem over the urban areas. This is likely due to the use of fractional land-use categories by the PX LSM in CMAQ which better accounts for urban heterogeneity, and thus, differing from the single dominant land-use category utilized by the Noah LSM in WRF/Chem.

Another process affecting surface $O_3$ distributions is dry deposition. MCIP (Otte and Pleim, 2010) was used to compute the $O_3$ dry deposition velocity ($V_{dO3}$) fields from relevant meteorological fields from WRF-for-CMAQ and WRF/Chem. Because $O_3$ dry deposition velocity was not part of the WRF/Chem August 2006 simulation output variable set, MCIP v3.4.1.1 was used to produce $V_{dO3}$. An earlier version of MCIP (v3.3) was used to process the WRF-for-CMAQ fields before the start of the

current study. Average afternoon $V_{dO3}$ and its differences between the two modeling systems (Fig. 8) partially support the $O_3$ differences in Fig. 3f. For example, where CMAQ has larger $O_3$ deposition velocity, such as along the Appalachians and the Alleghenies (Fig. 8c), WRF/Chem has more $O_3$ than CMAQ (Fig. 3f), and the converse is true in some areas near the southeast coast and in central Florida. However, other large areas of the field patterns of differences in Figs. 3f and 8c do not match, indicating that additional processes are responsible for the differences in simulated $O_3$.

MCIP also estimated total cloud fractional coverage from WRF-for-CMAQ and WRF/Chem, and their average afternoon values, with differences, are shown in Fig. 9. In general, WRF-for-CMAQ, with its Kain-Fritsch (KF) cumulus parameterization, produced more clouds in the afternoon than WRF/Chem with its Grell-Dévényi (GD) cumulus parameterization, with this difference being most pronounced in the South and the southwestern Plains (Fig. 9c). The influence of afternoon total cloud fraction is evident in the patterns for afternoon PBL heights for both WRF-for-CMAQ (comparing Figs. 9a and 7a) and WRF/Chem (comparing Figs. 9b and 7b), but is not readily seen in the afternoon surface $O_3$ patterns (Figs. 3d and e). An examination of MCIP-estimated cloud liquid water content and convective and nonconvective precipitation (not shown) also showed little influence on average surface $O_3$ patterns.

## 4. Examination of simulated ozone aloft

The near surface (i.e., lowest model layer) analyses and comparisons with surface measurements discussed thus far have not enabled us to provide adequate explanation of why the WRF/Chem August 2006 simulation shows more surface $O_3$ than CMAQ in the eastern U.S. while having a deeper PBL. Therefore, some examination of $O_3$ in the lower troposphere was conducted.

### *4.1. Ozone in the residual layer*

After sunset, radiative cooling forms a strong temperature inversion at the surface, effectively cutting off vertical mixing, thereby allowing deposition and chemical processes (primarily NO titration) at the surface to significantly reduce $O_3$ mixing ratios, often to just a few parts per billion. Ozone and other pollutants aloft from the afternoon mixed layer become trapped in the residual layer above the shallow nocturnal, or stable, boundary layer (SBL). Thus, the residual layer acts as an $O_3$ reservoir and provides a source for the next day's ground-level $O_3$ as mid-morning surface heating erodes away the SBL and initial daytime convection mixes $O_3$ from the residual layer down to the surface (Zhang and Rao, 1999). Average morning (11-14 UTC) $O_3$ aloft for August 2006 from both modeling systems and their differences (Fig. 10) at ~1100 m above ground level (AGL) (model layer 14) and a sampled west-east vertical cross section (model row 90) reveal that WRF/Chem has about 3-7 ppbv, or about 10%, more $O_3$ in the residual layer than CMAQ up to 2500 m AGL (model layer 20) over the central South, ORV, and Mid-Atlantic coast (Figs. 10c and f). Therefore, on average, WRF/Chem has more $O_3$ available over this area at the beginning of daytime mixing and $O_3$ production than CMAQ, and the stronger vertical mixing of WRF/Chem's YSU PBL scheme leads to greater entrainment (Hu et al., 2010) of $O_3$ aloft into the daytime mixed layer.

*4.2. Daytime ozone in the lower troposphere*

*4.2.1. Comparison with IONS-06 observations*

For comparison with upper air ozone, $O_3$ profile observations from the INTEX-B Ozonesonde Network Study 2006 (IONS-06; Thompson et al., 2008) were paired, both temporally and spatially, with instantaneous extracted model profiles from the CMAQ and WRF/Chem simulations for August 2006. Monthly mean and median $O_3$ profiles, and their standard deviations, were computed from all available matching profiles from 12 IONS-06 sites in the eastern U.S. domain. Because both models used the same boundary conditions, their $O_3$ profiles are generally similar, except within the daytime PBL where WRF/Chem had up to 5-20 ppbv more $O_3$ than CMAQ at some of the inland sites, such as Huntsville,

Alabama, and Beltsville, Maryland (Fig. 11). For this comparison, daytime profiles were separated from nocturnal profiles; the averaged profiles for Huntsville (Fig. 11a) consist of 29 daytime profiles, while the less-smooth averaged profiles for Beltsville (Fig. 11b) came from only six available daytime profiles. The CMAQ and WRF/Chem $O_3$ profiles are in somewhat better agreement (within 10 ppbv or less, and having similar profile shapes) when based on the six nocturnal and dawn profiles available from Beltsville for August 2006 (not shown). Compared to observations, both CMAQ and WRF/Chem tended to overestimate $O_3$ within the PBL at most sites, except for a 5-15 ppbv underprediction for Huntsville, Boulder, Colorado, and Bratt's Lake, Saskatchewan. In addition, both models had fairly uniform, underpredicted $O_3$ profiles above the PBL, with underpredictions of 20-40 ppbv in the middle troposphere increasing to 150-200 ppbv near the 100 hPa level (not shown).

*4.2.2. Modeled afternoon ozone*

Average August 2006 simulated afternoon $O_3$ aloft at selected levels, with differences, are shown in Fig. 12, which, when combined with the afternoon surface $O_3$ of Figs. 3d-e, illustrates the 3-D distribution of $O_3$ in the lower atmosphere. The influence of the stably stratified areas on the $O_3$ differences (i.e., where CMAQ $O_3$ is greater than WRF/Chem) decreases with height (Figs. 3f, 12f and c), but in the eastern U.S., CMAQ and WRF/Chem $O_3$ differences of 5-9 ppbv occur higher in the PBL as seen at ~1100 m AGL near the middle of the PBL (Fig. 12f). At slightly over 2 km AGL, afternoon $O_3$ mixing ratios have decreased (Figs. 12a and b) and differences in modeled $O_3$ have diminished to generally less than 3-5 ppbv (Fig. 12c). In particular, the selected west-east vertical cross section of simulated afternoon $O_3$ with differences (Fig. 13) also illustrates that WRF/Chem has more $O_3$ aloft than CMAQ in the upper portions of the afternoon mixed layer over areas with greater surface $O_3$ mixing ratios.

*4.3. Afternoon $J_{NO2}$ photolysis rates*

Analyses comparing the afternoon-averaged $NO_2$ photolysis rates ($J_{NO2}$) (Fig. 14), which include cloud effects, revealed that $J_{NO2}$ values from WRF/Chem using Fast-J increase with height more rapidly than $J_{NO2}$ values from CMAQ using JPROC/PHOT, especially over water in the Gulf of Mexico and the Atlantic Ocean off the SE coast where at ~2200 m AGL the WRF/Chem $J_{NO2}$ can be nearly double the $J_{NO2}$ in CMAQ (Fig. 14a-c). The sampled west-east vertical cross section of $J_{NO2}$ (Fig. 15) from both modeling systems shows that afternoon $J_{NO2}$ differences were greatest around 2-2.5 km AGL (Fig. 15c), then generally decrease with height above that. A comparison of modeled $J_{NO2}$ values aloft with measurements taken by the NOAA WP-3D Orion aircraft (P3) along a 31 August 2006 flight track from Tampa Bay, Florida, to the Houston, Texas, area is shown in Fig. 16. Cloud cover from Tropical Depression Ernesto (off the Georgia coast) affected the flight until ~19 UTC. After that, modeled $J_{NO2}$ values more closely follow observations under mostly clear skies, even during the aircraft ramp "profiles" around 19:50 and 21:15 UTC. The greater $J_{NO2}$ values aloft from WRF/Chem's Fast-J occur within clouds or between cloud layers (Wild et al., 2000) over areas with greater cloud liquid water content, whereas CMAQ's JPROC tables are only attenuated by clouds as a function of single-layer total cloud fraction (Roselle et al., 1999) without consideration of within-cloud scattering of radiation and interaction between multiple overlapping cloud layers. Real and Sartelet (2010) reported that the greatest photolysis rate differences occurred mainly within clouds in their comparison of attenuated clear-sky JPROC-generated tables and a newer version of the Fast-J scheme; in fact, the greater the cloud optical depth, the greater the photolysis rate differences between the offline and online photolysis schemes. Thus in this intercomparison, WRF/Chem's often greater photolysis rates aloft may be the primary reason for its greater average surface $O_3$ mixing ratios in the central South, ORV, and Mid-Atlantic when compared to CMAQ.

## 5. Conclusions

Air quality simulations were performed with the WRF-driven CMAQ and WRF/Chem for August 2006 using the same emissions, and initial and boundary conditions. Intercomparison of modeled gas phase chemistry was made more compatible by implementing the CB05 photochemical mechanism into WRF/Chem v3.0.1.1 and configuring the models to be as similar as practical, using recommended options where configuration differences were necessary. Simulated month-averaged ozone in the lower troposphere from the two AQ modeling systems was described and compared, along with observations, and processes that may be responsible for any $O_3$ differences were examined.

Both WRF-driven CMAQ and WRF/Chem air quality modeling systems generally overestimated surface ozone during August 2006, mainly in the central South and the Ohio River Valley, with a positive normalized mean bias in the range of 20-100+ %. WRF/Chem produced more $O_3$ than CMAQ despite having a generally deeper afternoon boundary layer of more aged air. Over regions where the simulated $O_3$ was biased high, WRF/Chem built up and maintained a reservoir of roughly 10% more $O_3$ aloft than CMAQ. The online Fast-J photolysis scheme used by WRF/Chem takes into account convective cloud optical properties, complex cloud layer structures, and within-cloud scattering of radiation which amplified photolysis rates critical to $O_3$ production compared to the simpler offline JPROC-based photolysis scheme of CMAQ. Differences between the LSMs (PX or Noah), vertical mixing and entrainment in boundary layer physics (ACM2 or YSU), dry deposition, and convective cloud schemes (KF or GD) all contributed to the presence of more $O_3$ in the WRF/Chem results than in the WRF-driven CMAQ results. However, the photolysis scheme (JPROC/PHOT or Fast-J) likely had the greatest impact on the modeled $O_3$.

Our findings confirm the importance of thoughtful selection of AQ modeling system configuration options. We demonstrated that subtle changes in model configurations can strongly influence the air quality predictions. When this study began, the online WRF-CMAQ modeling system (Mathur et al., 2010) was under active development. A shift in AQ modeling toward online systems is anticipated as scientific and technological advances permit. A similar study comparing the online WRF-

CMAQ (publicly available in Fall 2011) with updated WRF/Chem is planned to further inform developments of coupled meteorological-chemical modeling systems.

**Acknowledgements**

We would like to thank Chris Nolte, Rob Gilliam, Wyat Appel, Shawn Roselle, George Pouliot, Ken Schere, Jon Pleim, Golam Sarwar, Steve Howard, David Wong, and Jim Godowitch (U.S. EPA/ORD/NERL/AMAD) for their discussions during this study, Harald Stark and Ken Aikin (NOAA/ESRL/CSD) for the TexAQS II WP-3D airborne data, and Anne Thompson (The Pennsylvania State Univ.) for the IONS-06 data.

Although this paper has been reviewed and approved for publication by the U.S. Environmental Protection Agency, it does not reflect the views and policies of the Agency.

**References**

Ackermann, I.J., Hass, H., Memmesheimer, M., Ebel, A., Binkowski, F.S., Shankar, U., 1998. Modal aerosol dynamics model for Europe: development and first applications. Atmospheric Environment 32, 2981-2999.

Appel, K.W., Gilliam, R.C., Davis, N., Zubrow, A., Howard, S.C., 2011. Overview of the atmospheric model evaluation tool (AMET) v1.1 for evaluating meteorological and air quality models. Environmental Modelling & Software 26, 434-443.

Binkowski, F.S., Roselle, S.J., 2003. Models-3 Community Multiscale Air Quality (CMAQ) model aerosol component 1. Model description. Journal of Geophysical Research 108, 4183.

Byun, D., Schere, K.L., 2006. Review of the Governing Equations, Computational Algorithms, and Other Components of the Models-3 Community Multiscale Air Quality (CMAQ) Modeling System. Applied Mechanics Reviews 59, 51-77.

Chen, F., Dudhia, J., 2001. Coupling an advanced land surface–hydrology model with the Penn State–NCAR MM5 modeling system. Part I: model implementation and sensitivity. Monthly Weather Review 129, 569-585.

Chou, M.-D., Suarez, M.J., 1994. An efficient thermal infrared radiation parameterization for use in general circulation models, NASA Tech. Memo. 104606. Climate and Radiation Branch, Laboratory for Atmospheres, NASA/Goddard Space Flight Center.

Davis, J.M., Bhave, P.V., Foley, K.M., 2008. Parameterization of N2O5 reaction probabilities on the surface of particles containing ammonium, sulfate, and nitrate. Atmos. Chem. Phys. 8, 5295-5311.

Dudhia, J., 1989. Numerical study of convection observed during the Winter Monsoon Experiment using a mesoscale two-dimensional model. Journal of the Atmospheric Sciences 46, 3077–3107.

Eder, B., Kang, D., Mathur, R., Yu, S., Schere, K., 2006. An operational evaluation of the Eta-CMAQ air quality forecast model. Atmospheric Environment 40, 4894-4905.

Foley, K.M., Roselle, S.J., Appel, K.W., Bhave, P.V., Pleim, J.E., Otte, T.L., Mathur, R., Sarwar, G., Young, J.O., Gilliam, R.C., Nolte, C.G., Kelly, J.T., Gilliland, A.B., Bash, J.O., 2010. Incremental testing of the Community Multiscale Air Quality (CMAQ) modeling system version 4.7. Geoscientific Model Development 3, 205-226.

Gilliam, R.C., Pleim, J.E., 2010. Performance assessment of new land surface and planetary boundary layer physics in the WRF-ARW. Journal of Applied Meteorology and Climatology 49, 760-774.

Godowitch, J.M., Hogrefe, C., Rao, S.T., 2008. Diagnostic analyses of a regional air quality model: Changes in modeled processes affecting ozone and chemical-transport indicators from NOx point source emission reductions. Journal of Geophysical Research 113, D19303.

Grell, G.A., Dévényi, D., 2002. A generalized approach to parameterizing convection combining ensemble and data assimilation techniques. Geophysical Research Letters 29, 1693.

Grell, G.A., Peckham, S.E., Schmitz, R., McKeen, S.A., Frost, G., Skamarock, W.C., Eder, B., 2005. Fully coupled "online" chemistry within the WRF model. Atmospheric Environment 39, 6957-6975.

Hong, S.-Y., 2010. A new stable boundary-layer mixing scheme and its impact on the simulated East Asian summer monsoon. Quarterly Journal of the Royal Meteorological Society 136, 1481-1496.

Hong, S.-Y., Lim, J.-O.J., 2006. The WRF single-moment 6-class microphysics scheme (WSM6). Journal of the Korean Meteorological Society 42, 129-151.

Hong, S.-Y., Noh, Y., Dudhia, J., 2006. A new vertical diffusion package with an explicit treatment of entrainment processes. Monthly Weather Review 134, 2318-2341.

Hu, X.-M., Nielsen-Gammon, J.W., Zhang, F., 2010. Evaluation of three planetary boundary layer schemes in the WRF model. Journal of Applied Meteorology and Climatology 49, 1831-1844.

Kain, J.S., 2004. The Kain–Fritsch convective parameterization: an update. Journal of Applied Meteorology 43, 170-181.

Mathur, R., Pleim, J., Wong, D., Otte, T., Gilliam, R., Roselle, S., Young, J., Binkowski, F., Xiu, A., 2010. The WRF-CMAQ integrated on-line modeling system: development, testing, and initial applications, in: Steyn, D.G., Rao, S.T. (Eds.), Air Pollution Modeling and its Application XX. Springer, Dordrecht, pp. 155-159.

Mlawer, E.J., Taubman, S.J., Brown, P.D., Iacono, M.J., Clough, S.A., 1997. Radiative transfer for inhomogeneous atmospheres: RRTM, a validated correlated-k model for the longwave. Journal of Geophysical Research 102, 16663-16682.

Olszyna, K.J., Bailey, E.M., Simonaitis, R., Meagher, J.F., 1994. $O_3$ and $NO_y$ relationships at a rural site. Journal of Geophysical Research 99, 14557-14563.

Otte, T.L., Pleim, J.E., 2010. The Meteorology-Chemistry Interface Processor (MCIP) for the CMAQ modeling system: updates through MCIPv3.4.1. Geoscientific Model Development 3, 243-256.

Pleim, J.E., 2006. A simple, efficient solution of flux–profile relationships in the atmospheric surface layer. Journal of Applied Meteorology and Climatology 45, 341-347.

Pleim, J.E., 2007. A combined local and nonlocal closure model for the atmospheric boundary layer. Part I: model description and testing. Journal of Applied Meteorology and Climatology 46, 1383-1395.

Real, E., Sartelet, K., 2010. Modeling of photolysis rates over Europe: impact on chemical gaseous species and aerosols. Atmospheric Chemistry and Physics Discussions 10, 16691-16745.

Roselle, S.J., Schere, K.L., Pleim, J.E., Hanna, A.F., 1999. Photolysis rates for CMAQ, in: Byun, D.W., Ching, J.K.S. (Eds.), Science Algorithms of the EPA Models-3 Community Multiscale Air Quality (CMAQ) Modeling System. U.S. Environmental Protection Agency, Office of Research and Development, Washington, D.C., pp. 14-1 to 14-8.

Schell, B., Ackermann, I.J., Hass, H., Binkowski, F.S., Ebel, A., 2001. Modeling the formation of secondary organic aerosol within a comprehensive air quality model system. Journal of Geophysical Research 106, 28275-28293.

Skamarock, W.C., Klemp, J.B., 2008. A time-split nonhydrostatic atmospheric model for weather research and forecasting applications. Journal of Computational Physics 227, 3465-3485.

Skamarock, W.C., Klemp, J.B., Dudhia, J., Gill, D.O., Barker, D.M., Duda, M.G., Huang, X.-Y., Wang, W., Powers, J.G., 2008. A description of the Advanced Research WRF version 3. NCAR Technical Note NCAR/TN-475+STR. Available at: http://www.mmm.ucar.edu/wrf/users/docs/arw_v3.pdf.

Tao, W.-K., Simpson, J., McCumber, M., 1989. An ice-water saturation adjustment. Monthly Weather Review 117, 231-235.

Thompson, A.M., Yorks, J.E., Miller, S.K., Witte, J.C., Dougherty, K.M., Morris, G.A., Baumgardner, D., Ladino, L., Rappenglück, B., 2008. Tropospheric ozone sources and wave activity over Mexico City and Houston during MILAGRO/Intercontinental Transport Experiment (INTEX-B) Ozonesonde Network Study, 2006 (IONS-06). Atmospheric Chemistry and Physics 8, 5113-5125.

Trainer, M., Parrish, D.D., Buhr, M.P., Norton, R.B., Fehsenfeld, F.C., Anlauf, K.G., Bottenheim, J.W., Tang, Y.Z., Wiebe, H.A., Roberts, J.M., Tanner, R.L., Newman, L., Bowersox, V.C., Meagher, J.F., Olszyna, K.J., Rodgers, M.O., Wang, T., Berresheim, H., Demerjian, K.L., Roychowdhury, U.K., 1993. Correlations of ozone with $NO_y$ in photochemically aged air. Journal of Geophysical Research 98, 2917-2925.

Wild, O., Zhu, X., Prather, M.J., 2000. Fast-J: accurate simulation of in- and below-cloud photolysis in tropospheric chemical models. Journal of Atmospheric Chemistry 37, 245-282.

Xiu, A., Pleim, J.E., 2001. Development of a land surface model. Part I: application in a mesoscale meteorological model. Journal of Applied Meteorology 40, 192-209.

Yarwood, G., Rao, S., Yocke, M., Whitten, G.Z., 2005. Updates to the carbon bond chemical mechanism: CB05, Final Report to the U.S. EPA, RT-04-00675. Available at: http://www.camx.com/publ/pdfs/CB05_Final_Report_120805.pdf.

Zhang, J., Rao, S.T., 1999. The role of vertical mixing in the temporal evolution of ground-level ozone concentrations. Journal of Applied Meteorology 38, 1674-1691.

Zhang, Y., 2008. Online-coupled meteorology and chemistry models: history, current status, and outlook. Atmospheric Chemistry and Physics 8, 2895-2932.

Figure Captions

**Fig. 1.** Diurnal domain-wide hourly $O_3$ statistics for August 2006 for AQS observations (black solid line with crosses), CMAQ (blue dashed line with triangles), and WRF/Chem (red dashed line with plus signs). Lines with symbols represent the median $O_3$ mixing ratios, while the shaded box extremes represent the first and third quartiles.

**Fig. 2.** The top row shows August 2006 month-averaged modeled $O_3$ mixing ratios (ppbv) as filled contours from (a) CMAQ and (b) WRF/Chem with overlaid month-averaged AQS observations (filled circles), along with the $O_3$ difference field as (c) CMAQ – WRF/Chem. Month averages were computed from the 744 hourly values at each location for the 31 days of August. The bottom row shows the normalized mean bias (NMB in %) of the simulated $O_3$ at the AQS sites for (d) CMAQ and (e) WRF/Chem.

**Fig. 3.** Month-averaged $O_3$ for August 2006 comparing simulated values to observations when averaged over two different diurnal time periods. CMAQ results are shown in the left column (a and d), WRF/Chem results in the middle column (b and e), and CMAQ – WRF/Chem differences in the right column (c and f) for local morning (11-14 UTC, top row) and afternoon (17-20 UTC, bottom row) time periods. Appropriately averaged $O_3$ mixing ratios (ppbv) are shown as filled contours for the simulations and filled circles for the AQS observations.

**Fig. 4.** Ozone production efficiency (the slope of the dashed regression line) calculated for 10-17 LST for August 2006 from (a and d) SEARCH observations, (b and e) CMAQ, and (c and f) WRF/Chem at Centreville, Alabama (top row) and Birmingham, Alabama (bottom row). Each dot represents a bin average of 5% of available data values plotted with the standard deviation from the $O_3$ mean.

**Fig. 5.** Air mass photochemical age versus $NO_z$ calculated for 10-17 LST for August 2006 from (a and d) SEARCH observations, (b and e) CMAQ, and (c and f) WRF/Chem at Centreville, Alabama (top row) and Birmingham, Alabama (bottom row). Similar to Fig. 4, each dot represents a bin average of 5% of available data values plotted with the standard deviation from the $NO_z$ mean.

**Fig. 6.** Month-averaged August 2006 PBL height (m AGL) from (a) WRF-for-CMAQ and (b) WRF/Chem, and differences in meters (c) for WRF-for-CMAQ – WRF/Chem.

**Fig. 7.** August 2006 month-averaged local afternoon (17-20 UTC) PBL height (m AGL) and differences (m) from (a) WRF-for-CMAQ, (b) WRF/Chem, and (c) WRF-for-CMAQ – WRF/Chem.

**Fig. 8.** August 2006 month-averaged local afternoon (17-20 UTC) diagnosed dry deposition velocity (cm $s^{-1}$) for $O_3$ and differences (cm $s^{-1}$) from (a) WRF-for-CMAQ, (b) WRF/Chem, and (c) WRF-for-CMAQ – WRF/Chem.

**Fig. 9.** August 2006 month-averaged local afternoon (17-20 UTC) total cloud fraction and differences from (a) WRF-for-CMAQ, (b) WRF/Chem, and (c) WRF-for-CMAQ – WRF/Chem.

**Fig. 10.** Local morning (11-14 UTC) averaged $O_3$ mixing ratios (ppbv) and differences (ppbv) for August 2006 for $O_3$ aloft (model layer 14, ~1100 m AGL) (top row) and a vertical west-east cross section (model row 90) (bottom row) from (a and d) CMAQ, (b and e) WRF/Chem, and (c and f) CMAQ – WRF/Chem. The ordinate of the cross sections (d-f) is linear in layer number, which is not scaled to geophysical height.

**Fig. 11.** Averaged daytime median (solid) and mean (dashed) $O_3$ mixing ratio profiles (ppbv) from IONS-06 observations (black), CMAQ (red), and WRF/Chem (blue) for August 2006 at (a) Huntsville, Alabama, and (b) Beltsville, Maryland.

**Fig. 12.** Month-averaged local afternoon (17-20 UTC) $O_3$ aloft for August 2006 showing mixing ratios (ppbv) from CMAQ in the left column (a and d) and WRF/Chem in the middle column (b and e), and CMAQ – WRF/Chem differences (ppbv) in the right column (c and f) for model layer 19 (~2150-2200 m AGL; top row) and layer 14 (~1100 m AGL; bottom row).

**Fig. 13.** Vertical west-east cross sections (model row 90) of local afternoon (17-20 UTC) averaged $O_3$ mixing ratios (ppbv) and differences (ppbv) for August 2006 from (a) CMAQ, (b) WRF/Chem, and (c) CMAQ – WRF/Chem. As before, the cross section ordinate is linear in layer number.

**Fig. 14.** August 2006 month-averaged local afternoon (17-20 UTC) $NO_2$ photolysis rates ($J_{NO2}$) in the lower troposphere showing $J_{NO2}$ ($min^{-1}$) from CMAQ in the left column (a, d, and g) and WRF/Chem in the middle column (b, e, and h), and CMAQ – WRF/Chem $J_{NO2}$ differences ($min^{-1}$) in the right column (c, f, and i) for model layer 19 (~2150-2200 m AGL; top row), layer 14 (~1100 m AGL; middle row), and layer 1 (~35 m AGL; bottom row).
**Fig. 15.** Vertical west-east cross sections of local afternoon (17-20 UTC) averaged $J_{NO2}$ photolysis rates ($min^{-1}$) and differences ($min^{-1}$) for August 2006 from (a) CMAQ, (b) WRF/Chem, and (c) CMAQ – WRF/Chem for model row 90. As before, the cross section ordinate is linear in layer number.
**Fig. 16.** Observed and modeled $J_{NO2}$ photolysis rates ($min^{-1}$) along the P3 aircraft flight path of 31 August 2006 from Tampa Bay, Florida, along the Gulf Coast to the Houston, Texas, area. P3 observations (gray) are shown at the one-second data frequency, while the simulation results from CMAQ (red) and WRF/Chem (blue) show the expected step-like transitions from one volume-averaged grid cell to another. Refer to http://www.esrl.noaa.gov/csd/modeleval/tx06/p3/0831/ for altitude and map plots of the flight track.

Table Captions

**Table 1.** Air quality simulation configuration similarities.
**Table 2.** Air quality simulation configuration differences.
**Table 3.** Selected maximum 8-h average $O_3$ statistics from the one-month (August 2006) simulations when compared to AQS observations. Statistical metrics are as defined in Eder et al. (2006) and computed in AMET (Appel et al., 2011).

Table 1.

| Feature | Selected for both AQ simulations |
|---|---|
| **Domain** | Eastern U.S. on 12-km grid with 34 layers |
| **Domain top** | 100 hPa |
| **Initial and boundary conditions** | NAM for meteorology; CMAQ simulation on 36-km grid for chemistry |
| **Chemical mechanism** | CB05 (Yarwood et al., 2005) |
| **Emissions** | USEPA 2001 NEI projected to 2006, BEIS Ver. 3.13, and Mobile6 |
| **Longwave radiation** | RRTM (Mlawer et al., 1997) |
| **Nudging** | Grid (analysis) FDDA |
| **Surface updates** | SST, albedo, vegetative fraction |
| **Land-use classification** | USGS |
| **Topographic effects** | Slope and topographic shading on radiation |
| **Eddy coefficient** | Horizontal Smagorinsky first-order closure |
| **Subgrid transport** | Subgrid convective chemistry transport |

Table 2.

| Feature | WRF and CMAQ | WRF/Chem |
|---|---|---|
| **Microphysics** | WSM 6-class (Hong and Lim, 2006) | Purdue Lin (Tao et al., 1989) |
| **Shortwave radiation** | Dudhia (Dudhia, 1989) | Goddard (Chou and Suarez, 1994) |
| **Surface layer physics** | Pleim (Pleim, 2006) | Monin-Obukhov (Skamarock et al., 2008) |
| **Land surface model** | Pleim-Xiu (Xiu and Pleim, 2001) | Noah (Chen and Dudhia, 2001) |
| **Planetary boundary layer** | ACM2 (Pleim, 2007) | YSU (Hong et al., 2006; Hong, 2010) |
| **Cumulus parameterization** | Kain-Fritsch (Kain, 2004) | Grell-Dévényi (Grell and Dévényi, 2002) |
| **Vertical velocity damping** | no | yes |
| **Positive-definite advection** | moisture, chemistry | moisture, scalars, chemistry |
| **Photolysis** | JPROC/PHOT (Roselle et al., 1999) | Fast-J (Wild et al., 2000) |
| **Aerosols** | AE4 with updated $N_2O_5$ gamma parameterization (Binkowski and Roselle, 2003; Davis et al., 2008) | MADE/SORGAM (Ackermann et al., 1998; Schell et al., 2001) |

Table 3.

| Max. 8-h Avg. $O_3$ Statistic | CMAQ | WRF/Chem |
|---|---|---|
| **Root Mean Square Error (RMSE) (ppbv)** | 11.52 | 13.57 |
| **Normalized Mean Error (NME) (%)** | 18.2 | 21.5 |
| **Mean Bias (MB) (ppbv)** | 3.62 | 6.18 |
| **Normalized Mean Bias (NMB) (%)** | 7.4 | 12.7 |
| **Correlation coeff. (r)** | 0.72 | 0.66 |

Figure 1.

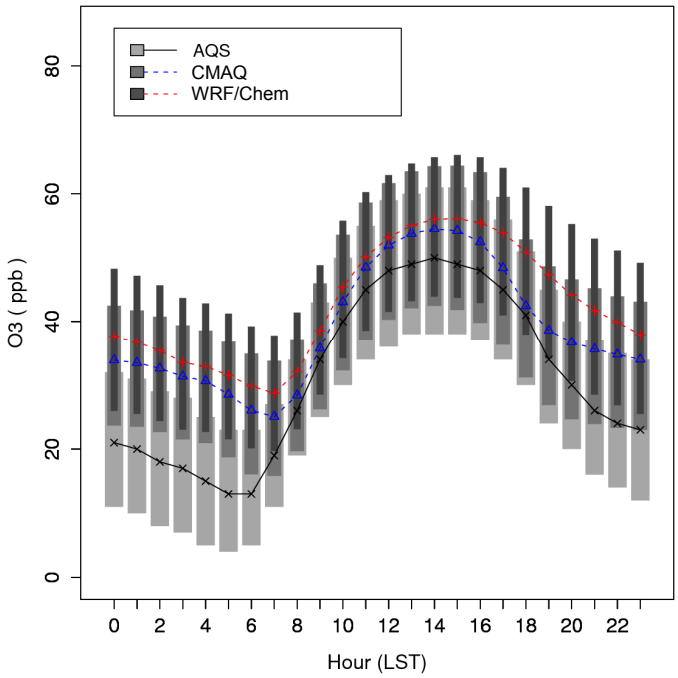


Figure 2.

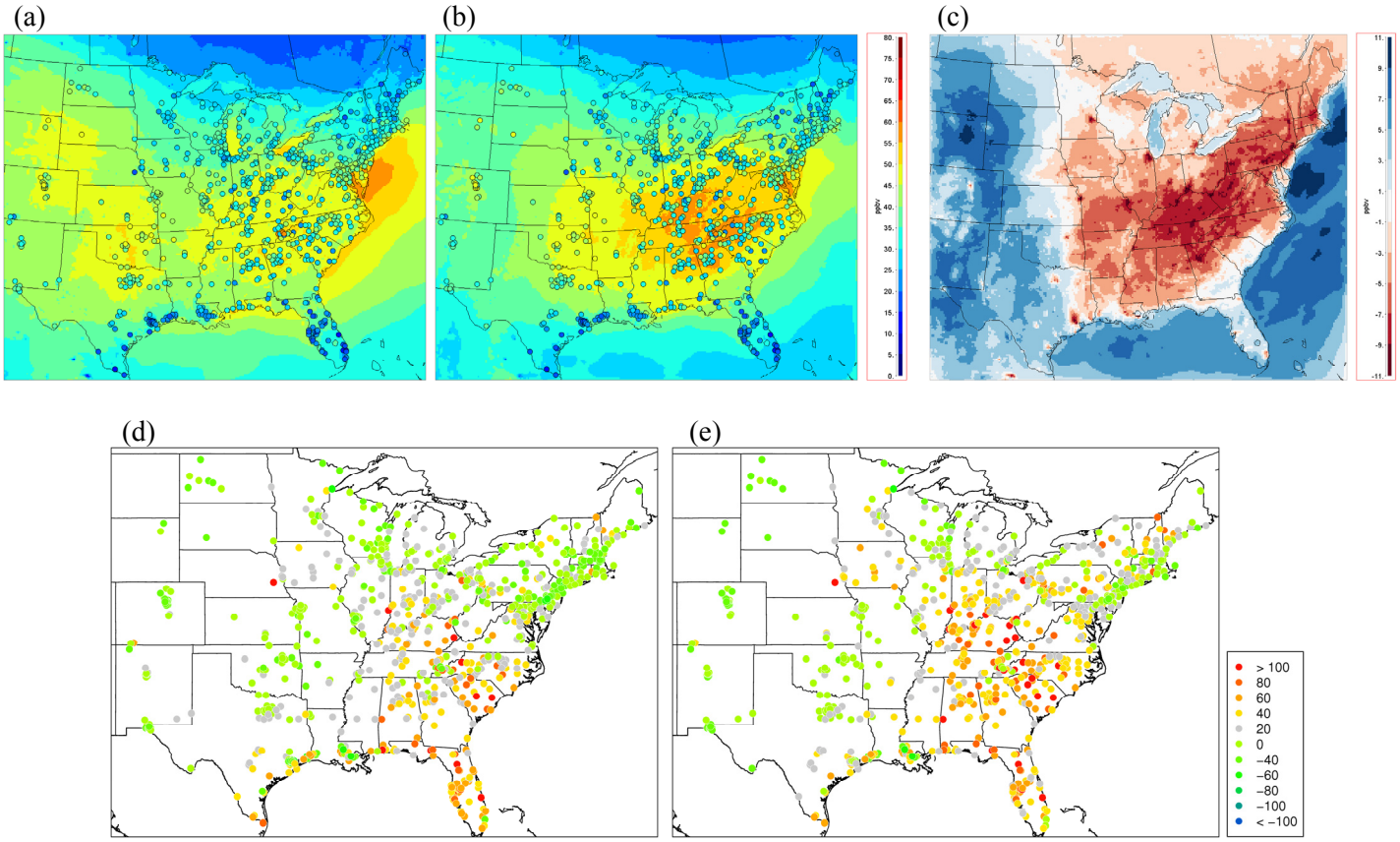

Figure 3.

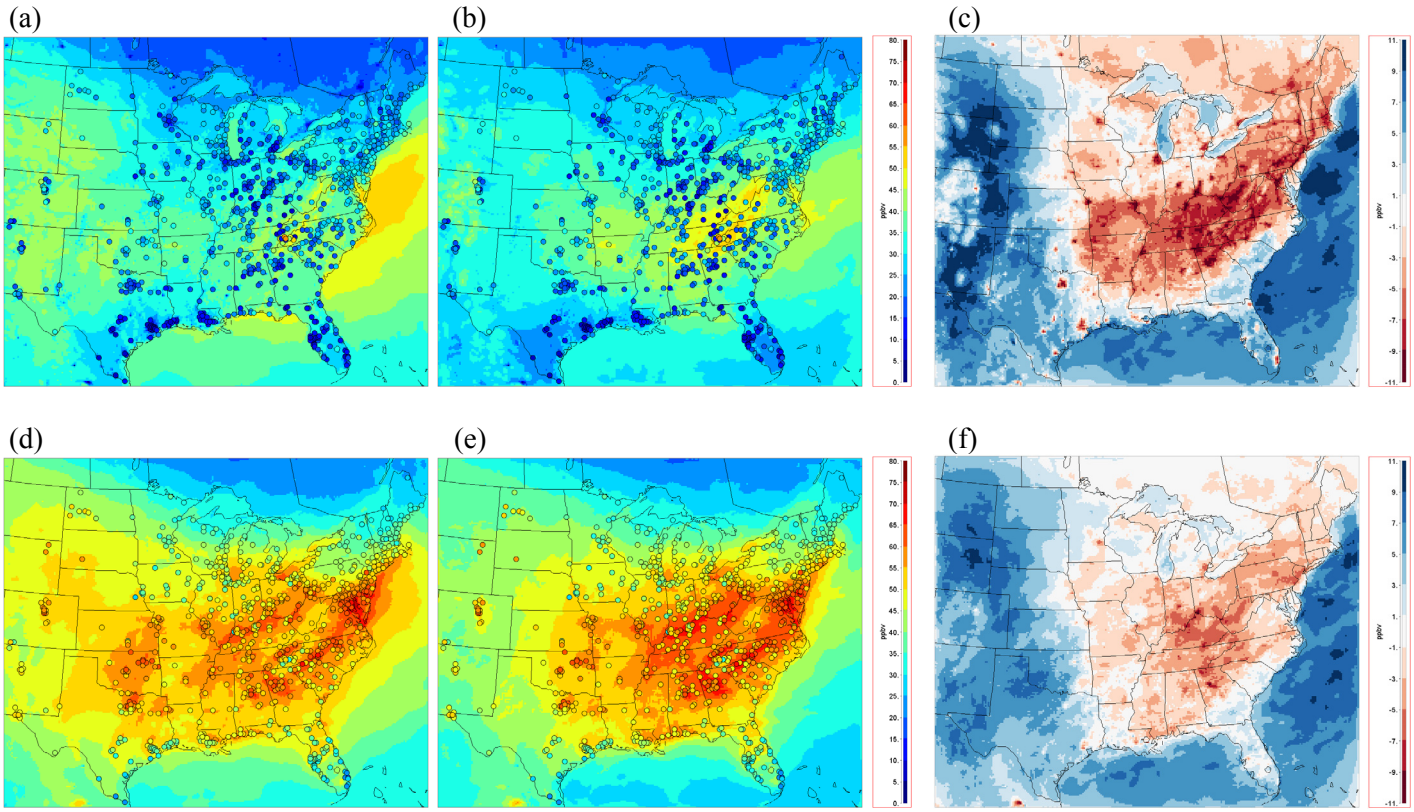


Figure 4.

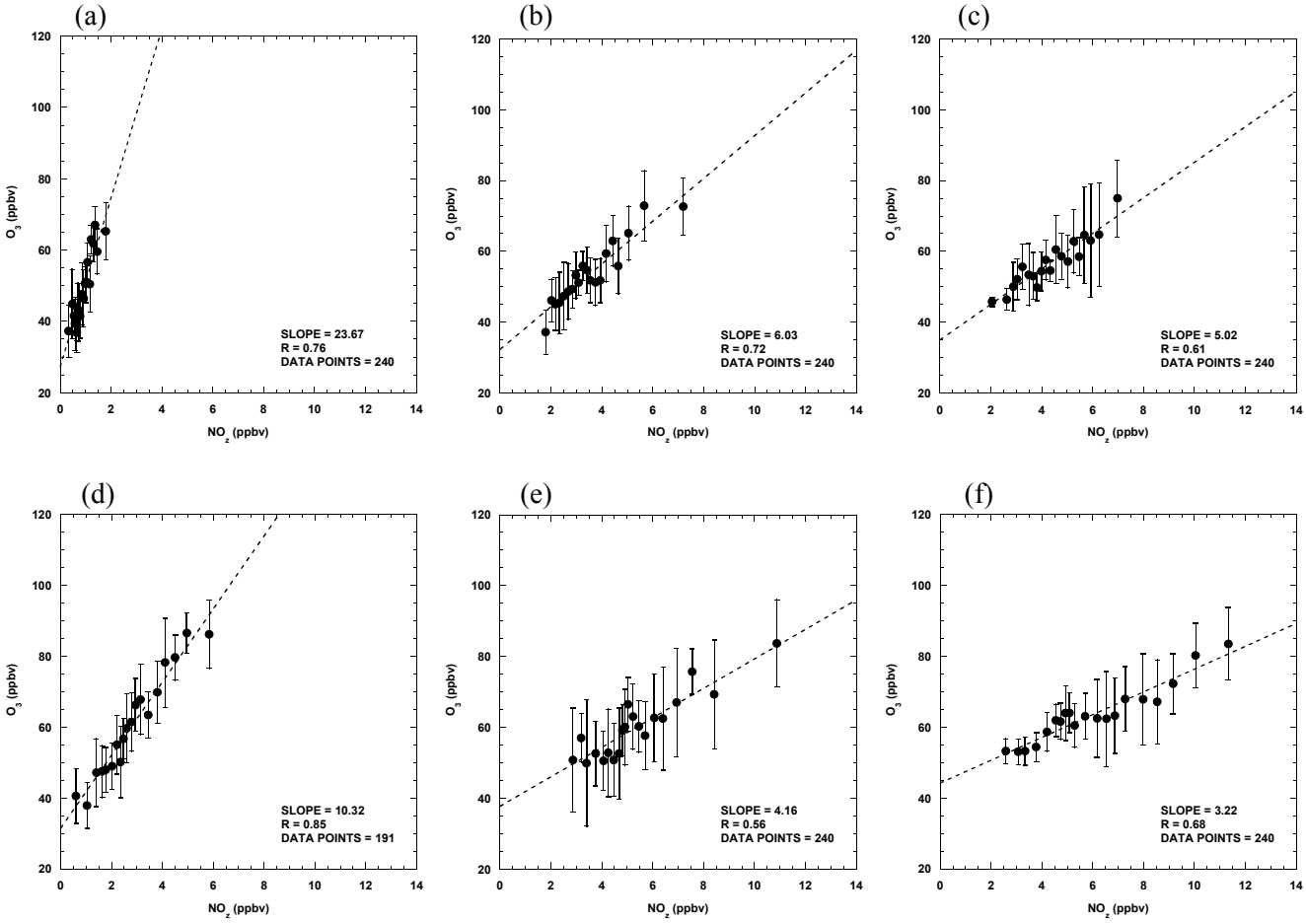

Figure 5.

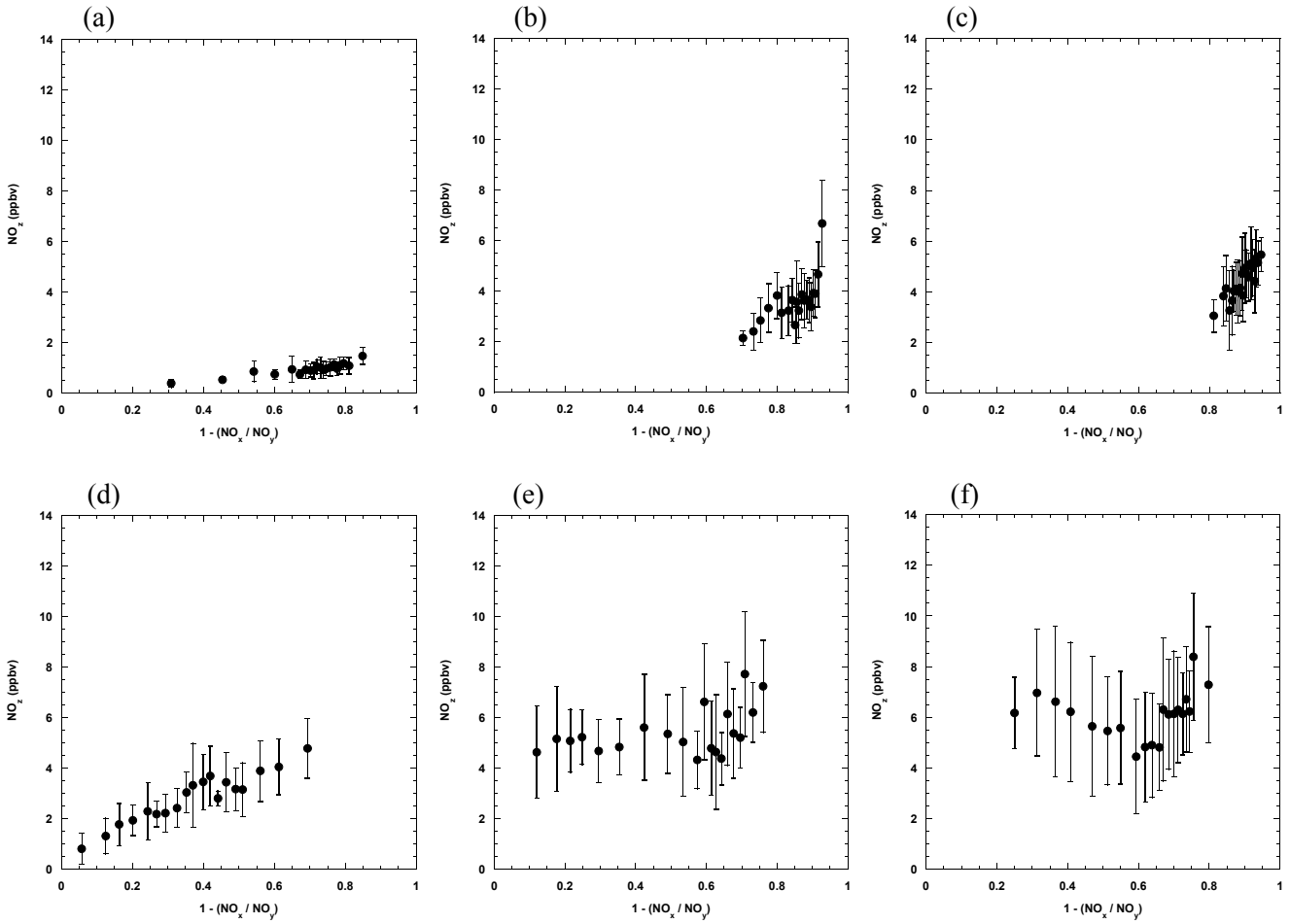


Figure 6.

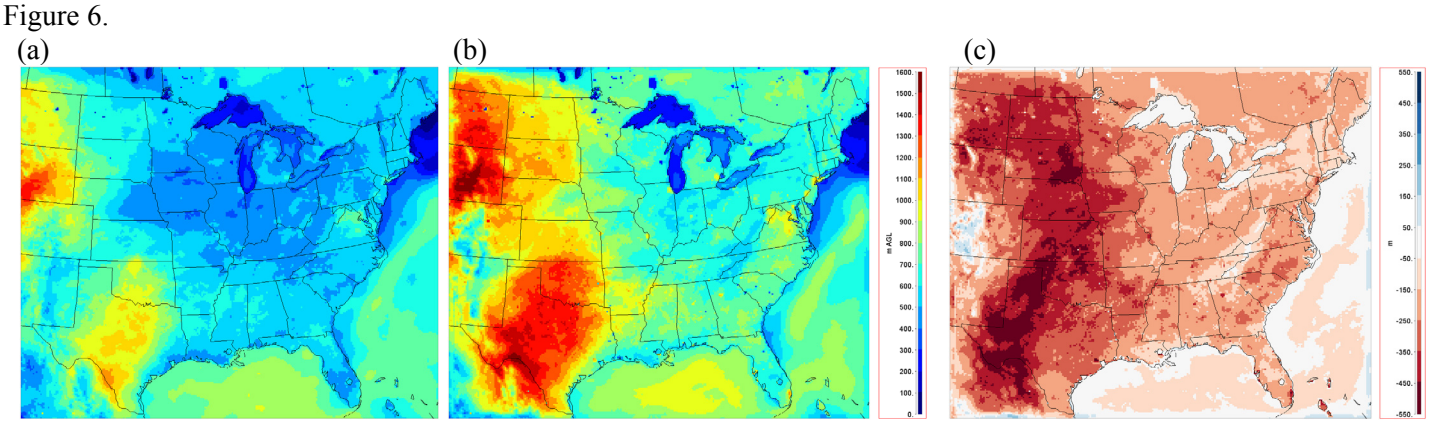

Figure 7.

(a) (b) (c)

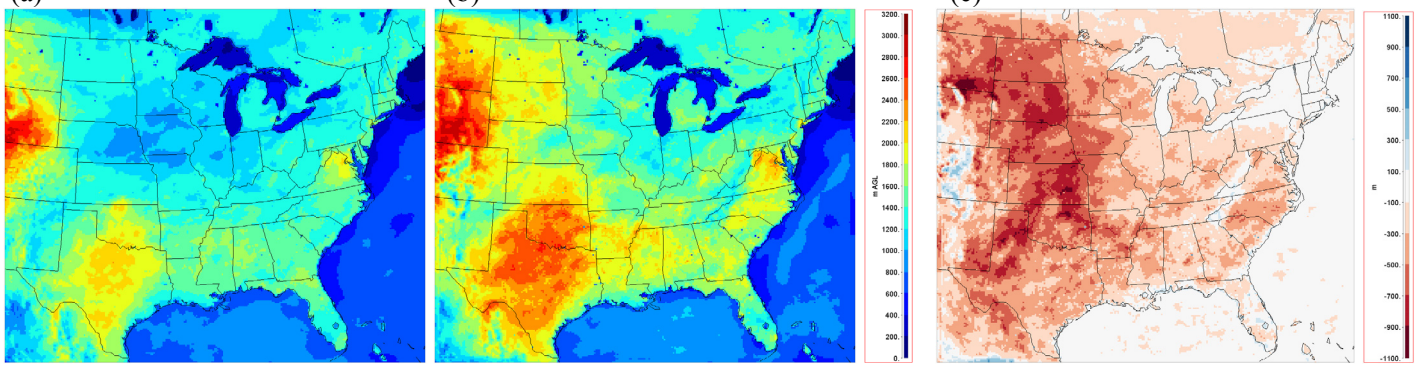


Figure 8.

(a) (b) (c)

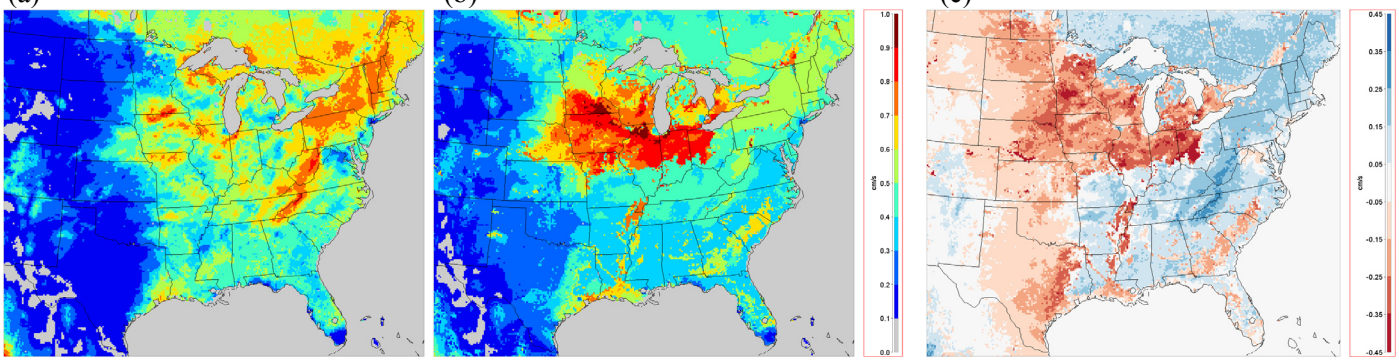


Figure 9.

(a) (b) (c)

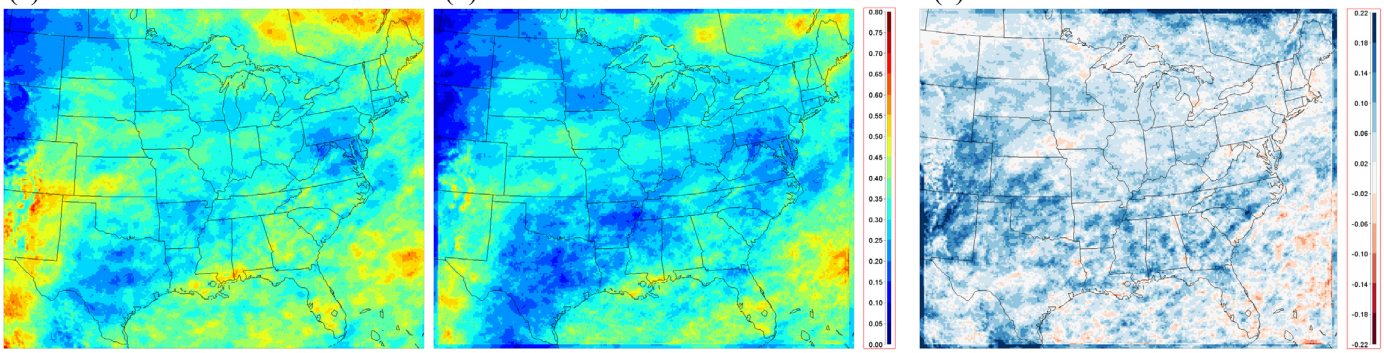

Figure 10.

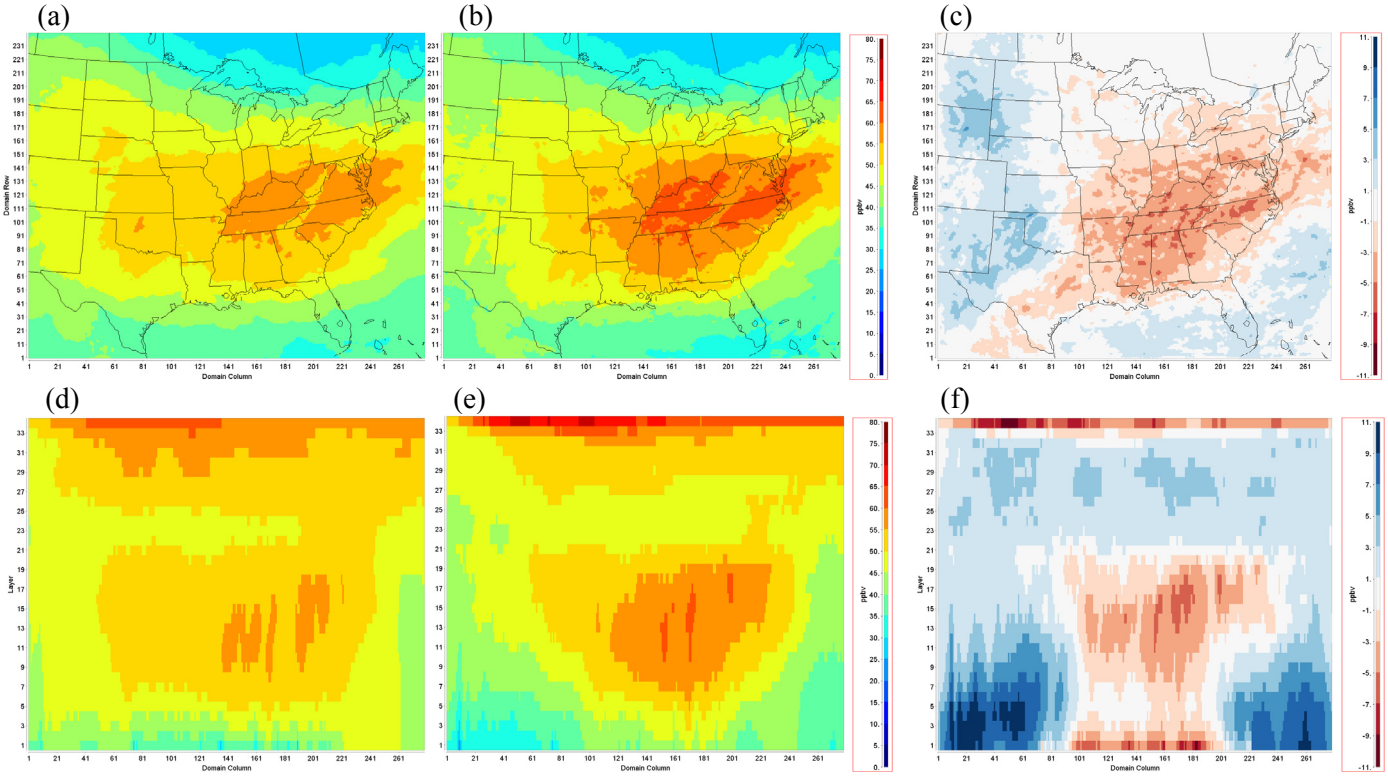


Figure 11.

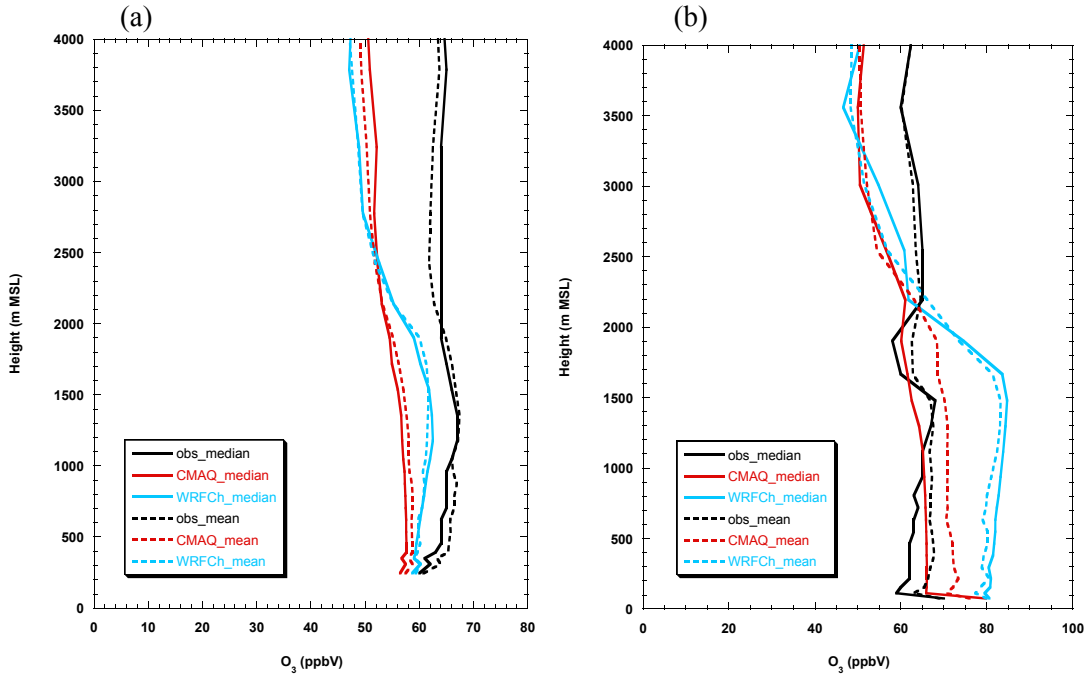

Figure 12.

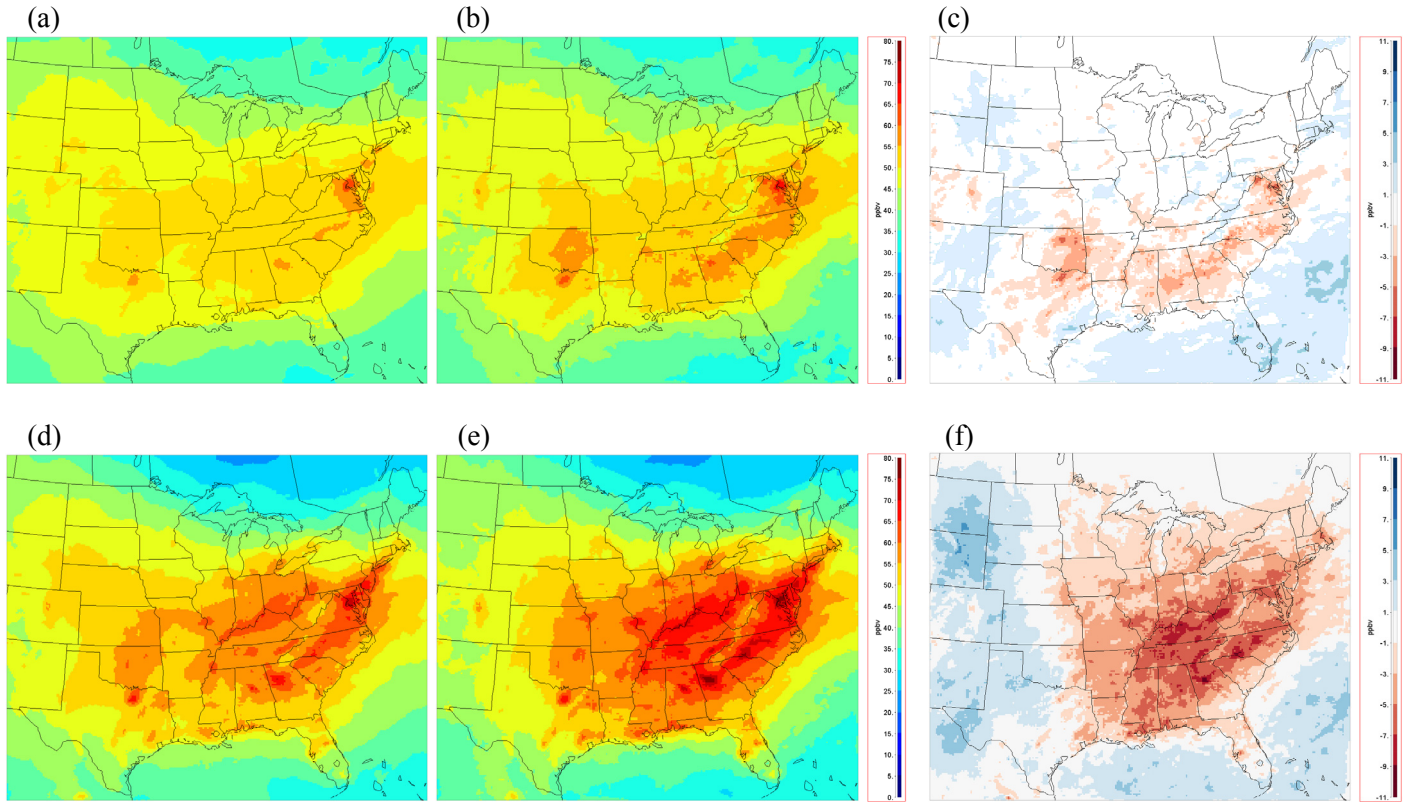


Figure 13.

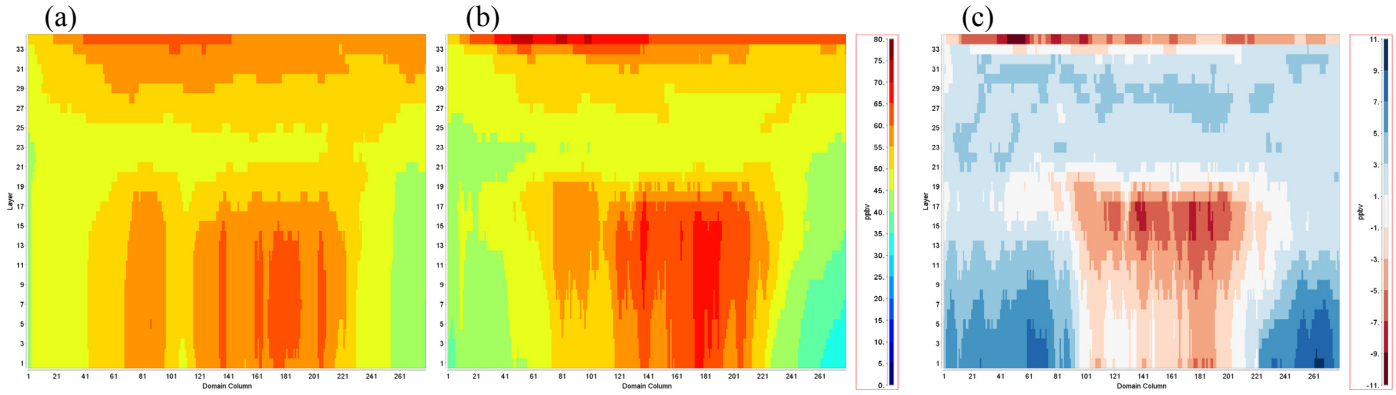

Figure 14.

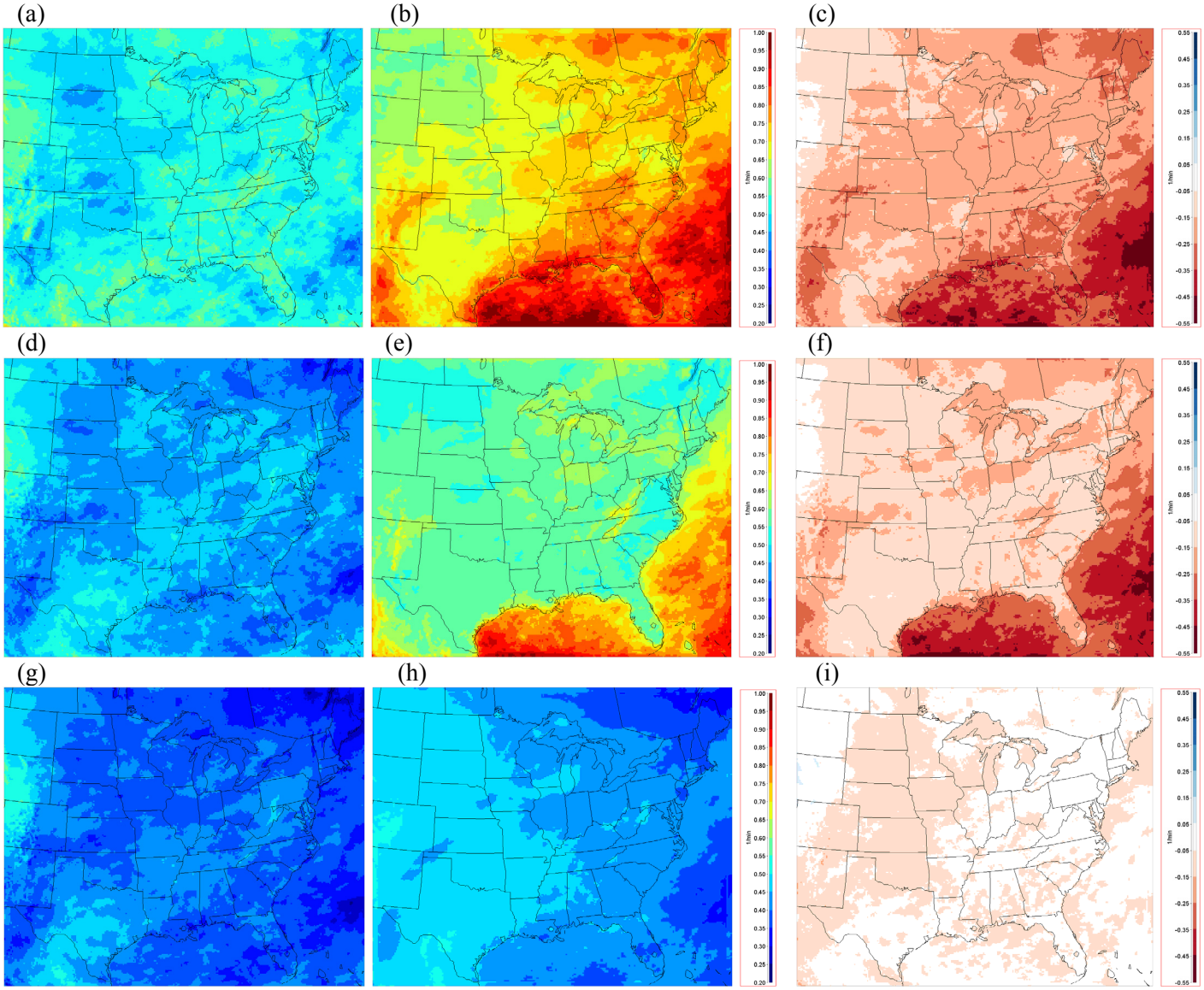


Figure 15.

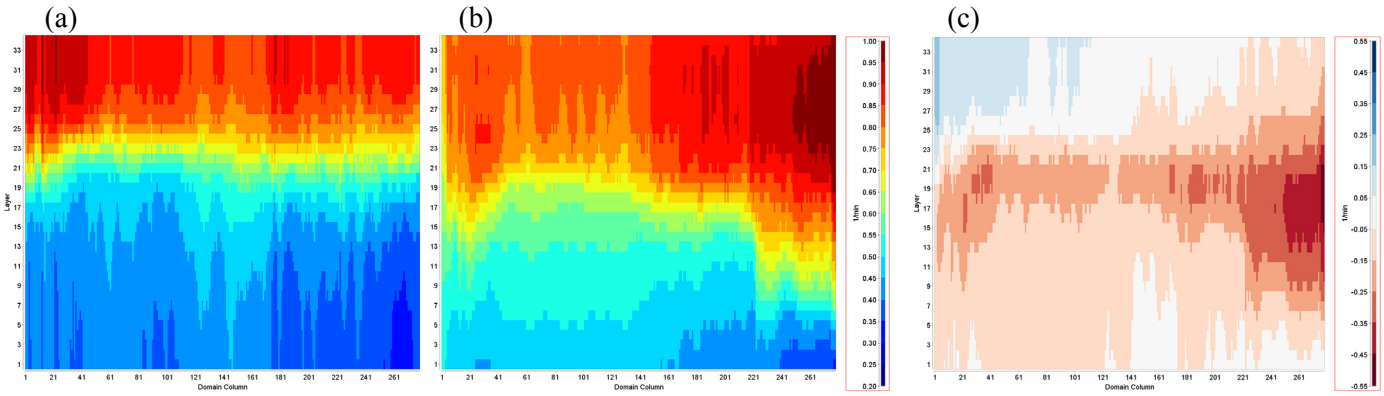

Figure 16.

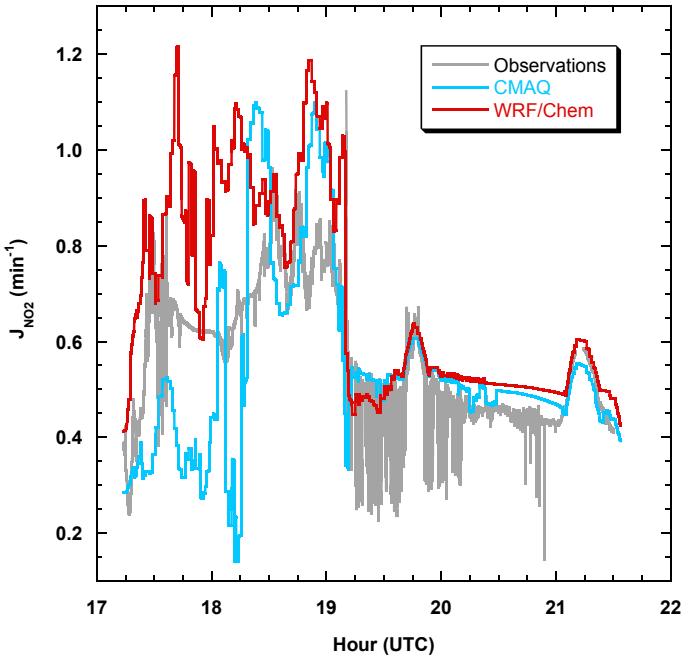
Observations
CMAQ
WRF/Chem
1.2
1.0
0.8
0.6
0.4
0.2
$J_{NO2}$ (min$^{-1}$)
17
18
19
20
21
22
Hour (UTC)